







# Preferential Heating of Protons over Electrons from Coherent Structures during the First Perihelion of the Parker Solar Probe

Nikos Sioulas , Chen Shi (时辰) , Zesen Huang (黄泽森) , and Marco Velli   
Department of Earth, Planetary, and Space Sciences, University of California, Los Angeles, CA 90095, USA  
Received 2022 June 21; revised 2022 August 1; accepted 2022 August 2; published 2022 August 18

## Abstract

The solar wind undergoes significant heating as it propagates away from the Sun; the exact mechanisms responsible for this heating remain unclear. Using data from the first perihelion of the Parker Solar Probe mission, we examine the properties of proton and electron heating occurring within magnetic coherent structures identified by means of the Partial Variance of Increments (PVI) method. Statistically, regions of space with strong gradients in the magnetic field,  $PVI \geq 1$ , are associated with strongly enhanced proton but only slightly elevated electron temperatures. Our analysis indicates a heating mechanism in the nascent solar wind environment facilitated by a nonlinear turbulent cascade that preferentially heats protons over electrons.

*Unified Astronomy Thesaurus concepts:* [Solar wind \(1534\)](#); [Solar coronal heating \(1989\)](#); [Interplanetary turbulence \(830\)](#); [Magnetohydrodynamics \(1964\)](#)

## 1. Introduction

Within the inner heliosphere, the ion temperature of the solar wind decays as a function of radial distance as  $T_p \sim r^{-\gamma_p}$ , where  $0.5 \lesssim \gamma_p \lesssim 1$ , (Richardson et al. 1995; Stansby et al. 2018), while the electron temperature decays as  $T_e \sim r^{-\gamma_e}$ , where  $0.3 \lesssim \gamma_e \lesssim 0.7$  (Maksimovic et al. 2005; Boldyrev et al. 2020). As a result, the electron and proton temperatures of the solar wind decay at much slower rates than predicted by spherically symmetric adiabatic expansion models (i.e.,  $T \sim r^{-4/3}$ ). In order to fully understand solar wind dynamics, supplementary heating processes must be considered (Matthaeus & Velli 2011). In recent years, a multitude of mechanisms for transferring turbulent energy into thermal degrees of freedom in weakly collisional plasmas have been explored, including wave–particle interactions (Isenberg & Hollweg 1983; Leamon et al. 1999; Bourouaine et al. 2012; González et al. 2021) and nonresonant mechanisms such as stochastic heating (Chandran et al. 2010; Bourouaine & Chandran 2013). Another potential source of nonadiabatic heating is the magnetohydrodynamic turbulence in the solar wind (Coleman 1968). In particular, observational and numerical studies indicate that plasma heating occurs in an intermittent fashion and suggest a statistical link between coherent magnetic field structures (CSs) and elevated temperatures (Osman et al. 2012; Chasapis et al. 2015; Yordanova et al. 2021; Sioulas et al. 2022a, 2022b). The intermittent character of turbulence can be attributed to a fractally distributed population of small-scale CSs, superposed on a background of random fluctuations that, despite occupying only a minor fraction of the entire data set (Vlahos et al. 2008; Parashar et al. 2009; Osman et al. 2012; Wan et al. 2012; Sioulas et al. 2022a, 2022b) can account for a disproportionate amount of magnetic energy dissipation and heating of charged particles (Karimabadi et al. 2013; Sioulas et al. 2020a, 2020b; Bandyopadhyay et al. 2020).

It is essential that the dominant heating mechanism(s) is (are) consistent with a broad range of in situ, as well as remote, observations, including the following: (1) The heating must be spatially extended out to several solar radii in order to drive observed wind speeds, (2) the preferential heating of protons is in the direction perpendicular to the magnetic field, and (3) protons are preferentially heated over electrons, with heavier ion heating being even more pronounced.

In this study, we aim to investigate proton versus electron heating in the nascent solar wind environment. For this reason, we analyze the Quasi-Thermal Noise (QTN) electron data and proton data from the Solar Probe Analyzer (SPAN) part of the Solar Wind Electron, Alpha, and Proton (SWEAP) suite (Kasper et al. 2016) during the first encounter of the Parker Solar Probe mission (PSP) with the Sun (Fox et al. 2016). As a first step, we utilize the Partial Variance of Increments (PVI) method to identify the underlying coherent structures in our data set. Subsequently, we carry out a superposed-epoch analysis to study the effects of CSs on charged particle heating. We show that both ions and electrons are heated in the vicinity of CSs; however, the effect is considerably less efficient for electrons. The structure of this paper is as follows: Section 2 describes the PVI methods, the diagnostic used in this study to identify coherent structures, and Section 3 presents the selected data and their processing. In Section 4 we present the results of this study. Section 5 provides a summary of the results and conclusions.

## 2. Background

Since the beginning of in situ observations, it has been revealed that several types of localized coherent structures abound in the solar wind (Hudson 1971; Tsurutani & Smith 1979). A number of recent studies suggest that CSs are dynamically generated as a by-product of the turbulent cascade (Matthaeus & Lamkin 1986; Veltri 1999; Sioulas et al. 2022), or/and are of coronal origin being passively advected by the solar wind (Borovsky 2021). The borders of such structures have been shown to remain in a dynamic state and have been associated with strong gradients in turbulent fields, resulting in local nonlinear interactions and processes such as

magnetic reconnection or various types of instabilities (Matthaeus et al. 2015). The PVI method is an analytical tool for detecting sharp gradients in a turbulent field and can be estimated as (Greco et al. 2008)

$$PVI(t, \tau) = \frac{|\delta \mathbf{B}(t, \tau)|}{\sqrt{\langle |\delta \mathbf{B}(t, \tau)|^2 \rangle}}, \quad (1)$$

where  $|\Delta \mathbf{B}(t, \tau)| = |\mathbf{B}(t + \tau) - \mathbf{B}(t)|$  is the magnitude of the magnetic field vector increments and  $\langle \dots \rangle$  represents the average over a large window, which is a multiple of the estimated magnetic field correlation time. As the PVI index increases, the identified events are more likely to be associated with non-Gaussian structures that lie on the “heavy tails” observed in the probability distribution function (PDF) of scale-dependent increments, suggesting that coherent structures correspond to events of index  $PVI \geq 2.5$ . The most intense magnetic field discontinuities, such as current sheets and reconnection sites, can then be identified by further raising the threshold value to  $PVI \geq 4$  and  $PVI \geq 6$ , respectively (Servidio et al. 2009).

### 3. Data and Analysis Procedure

We have analyzed data from the first encounter E1 of PSP with the Sun, during the period of 2018 November 1–November 10. For magnetic field measurements, in order to obtain high-quality data without interference from instrumental noise, which could lead to an artificial flattening of the power spectrum at the highest frequencies, we use the SCAm data product, which merges fluxgate and search-coil magnetometer (SCM) measurements from the FIELDS instrument (Bale et al. 2016) by making use of frequency-dependent merging coefficients, thus enabling magnetic field observations from DC to 1 MHz with an optimal signal-to-noise ratio (Bowen et al. 2020). Proton data were obtained from the SWEAP suite (Kasper et al. 2016), and electron data were derived from the quasi-thermal noise from the FIELDS instrument (Moncuquet et al. 2020). Note that the same electron analysis was repeated by taking into account core temperature data fitted from the SPAN-e electron VDFS (Halekas et al. 2020), with qualitatively similar results.

In order to estimate the PVI time series, SCAm magnetic field data have been linearly interpolated to a cadence of  $\delta\tau = 0.05$  s. Subsequently, following Equation (1), the PVI time series was estimated using an averaging window of duration  $d = 8$  hr, which was several times the estimated correlation time of the magnetic field for E1 of PSP (Chhiber et al. 2020). A lag of  $\delta\tau = 0.05$  s was used in estimating the PVI time series. Based on Taylor’s hypothesis, we can convert the temporal to spatial lag. We can then estimate the time-to-time ratio of the spatial lag to the ion inertial length to obtain the mean value of the spatial lag in units of the ion inertial length ( $d_i$ ). The obtained  $d_i$  time series, not shown here, is in agreement with Parashar et al. (2020). Therefore, the mean value of the spatial lag normalized in units of the  $d_i$  value corresponds to  $\bar{\ell} \approx 0.76 d_i$ , with a standard deviation of  $\pm 0.18 d_i$ . Note that the analysis was also carried out for various averaging times (from 1 to 12 hr), and it was observed to have minimal impact on the final result. Finally, the PVI time series was resampled to the electron time-series cadence of 7 s and proton time-series cadence of  $\sim 28$  s in such a way that for each interval, the mean value of PVI in that interval was chosen. Note that the same analysis was repeated by choosing

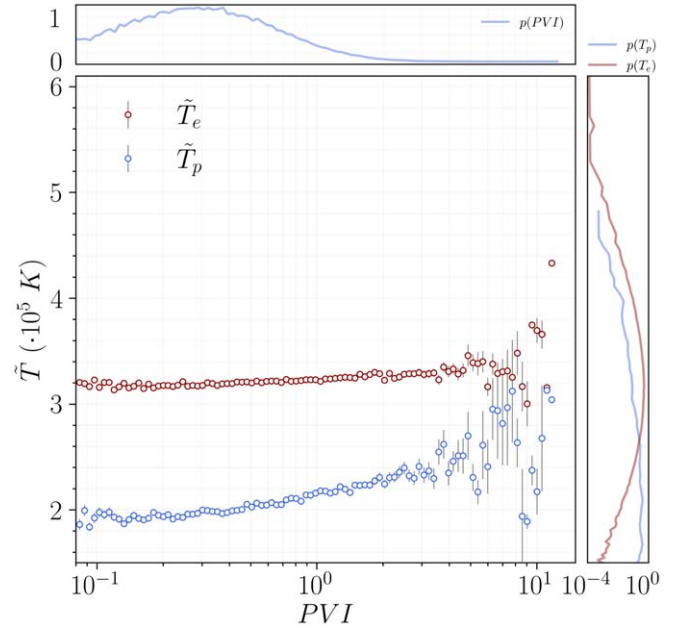


**Figure 1.** Binned mean of proton ( $T_p$  in blue) and electron temperatures ( $T_e$  in red) plotted against PVI. Error bars are also shown indicating the standard error of the mean,  $\sigma_i/\sqrt{n}$ , where  $\sigma_i$  is the standard deviation of the samples inside the bin. The PDFs of the electron and proton temperature  $p(T_e)$  and  $p(T_p)$ , and the PVI index  $p(PVI)$  are shown separately in red and blue on the top and right margins of the plot, respectively.

the maximum value of PVI within each interval with qualitatively similar results. Additionally, the lower-resolution data for the proton time series do not affect the final conclusion of this work, as the results presented here are in agreement with Sioulas et al. (2022b), who studied the correlation between PVI and proton temperature for the first six encounters of PSP using high-resolution (0.873 s) proton data from the Solar Probe Cup Instrument (SPC) data (Kasper et al. 2016).

### 4. Results

In this section, we investigate the contribution of coherent structures, identified by means of the PVI method (see Section 3), to the heating of protons and electrons in the solar wind. The first step in this analysis is to interpret  $T_p$  as a function of PVI through binned statistics. Figure 1 shows the average proton (blue) and electron (red) temperature per bin using 100 PVI bins (i.e.,  $\langle T_p(\theta_i \leq PVI \leq \theta_{i+1}) \rangle$ , where  $\theta_i$  is the PVI threshold) plotted against the center of the bin. Uncertainty bars are also shown, indicating the standard error of the sample (Gurland & Tripathi 1971). In this case, the uncertainty is estimated as  $\sigma_i/\sqrt{n}$ , where  $\sigma_i$  is the standard deviation of the samples inside the bin. The PDFs of the electron and proton temperatures  $p(T_e)$  and  $p(T_p)$ , as well as the PDF of the PVI index  $p(PVI)$  are shown separately in blue and red on the top and right margins of the plot. In agreement with previous studies (Osman et al. 2012; Yordanova et al. 2021; Sioulas et al. 2022a), a statistically significant positive correlation is observed with a high PVI index and elevated  $T_p$ . Nevertheless, the limited number of observations for  $PVI \geq 4$  results in the high variability of  $T_p$  on the right-hand side of the figure. More specifically, the lowest observed PVI values,  $PVI \sim 10^{-1}$ , are associated with a proton temperature of  $T_p \sim 4 \cdot 10^5$  K, while for  $PVI \sim 4$ , the proton temperature raises to  $T_p \sim 4.6 \cdot 10^5$  K. On the other hand, for electrons, only a moderate positive

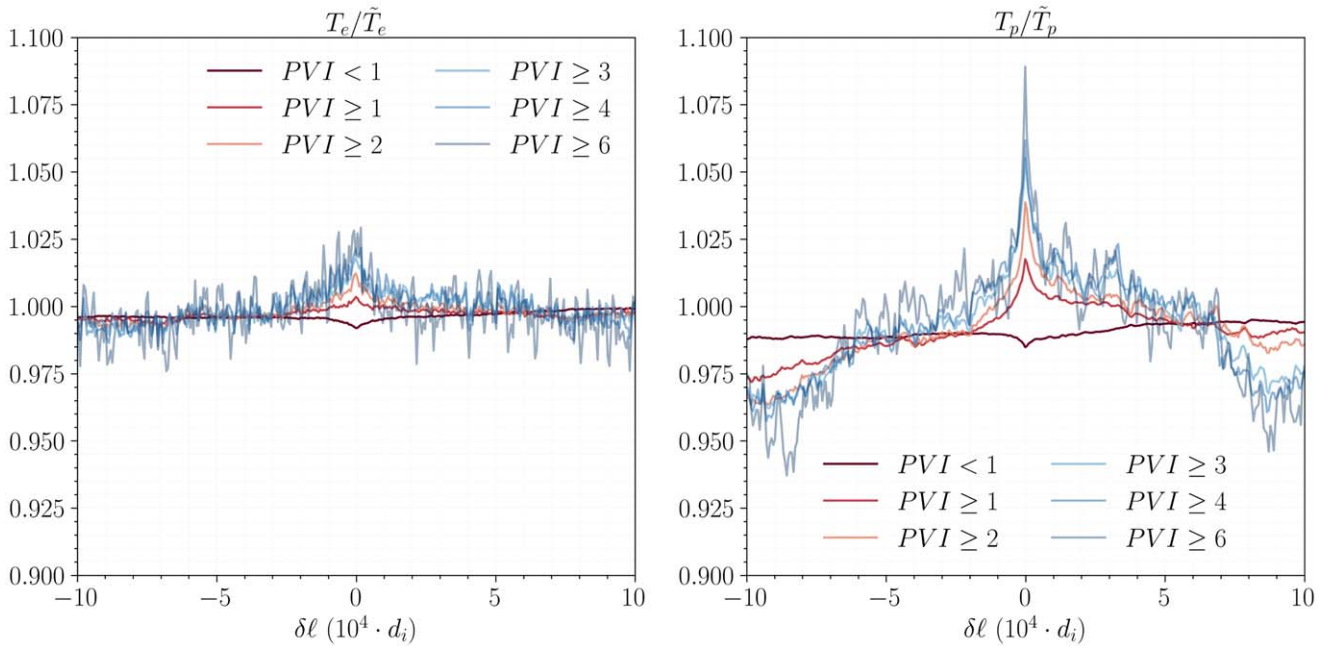


**Figure 2.** Average (a)  $T_e$  and (b)  $T_p$  conditioned on the spatial lag, normalized to the ion inertial length  $d_i$ , estimated separation from PVI events that exceed a PVI threshold. Note that  $T_j$ ,  $j = e, p$  has been normalized by the average value  $\tilde{T}_j$  within a window that spans  $\delta\ell = 2 \cdot 10^5 d_i$  and is centered around the discontinuity under study.

statistical correlation is observed. In particular, coherent structures characterized by a PVI index  $\text{PVI} \leq 1$ , hardly change the electron temperature, while for higher PVI thresholds, a rough statistical trend is observed. Note that several bins with  $\text{PVI} \sim 10$ , usually associated with reconnection exhausts (Servidio et al. 2012), display considerably increased electron temperatures  $T_e \geq 3.5 \cdot 10^5$  K. This could indicate that magnetic reconnection plays a major role in the electron heating observed in the solar wind. However, further study is needed to identify these structures and determine whether magnetic reconnection is indeed responsible for the observed heating, and whether other mechanisms are involved.

To gain a deeper understanding of the relationship between the temperature of the solar wind and magnetic field discontinuities, we estimate averages of  $T_j$ , where  $j = e$  and  $p$ , the temperature of electrons and protons respectively, constrained by the temporal separation between PVI events that belong to a given PVI bin. This can be formally expressed as (Tessein et al. 2013; Sorriso-Valvo et al. 2018)

$$\langle T_j(\Delta t, \theta_i, \theta_{i+1}) \rangle = \langle T_j(t_{\text{PVI}} + \Delta t) | \text{PVI} \geq \theta_i \rangle, \quad (2)$$

where  $\Delta t$  is the temporal lag relative to the location of the main PVI event taking place at time  $t_{\text{PVI}}$ , and  $\theta = [0, 1, 2, 3, 4, 6]$ . Figure 2 illustrates the conditional average of the electron and proton temperatures in the left and right panels, respectively, at different spatial lags. Note that temporal lags have been converted to spatial lags, subject to the validity of Taylor’s hypothesis (Taylor 1938),  $\ell = V_{\text{SW}}\Delta t$ . For a direct comparison between different plasma environments and to cast our results in physically relevant units, spatial scales have been normalized by the ion inertial length  $d_i = V_A/\Omega_i$ , where  $\Omega_i = \frac{eB}{m_p}$  is the proton gyrofrequency,  $e$  is the elementary charge,  $B$  is the mean magnetic field, and  $m_p$  is the mass of the proton (Huba 2004). Additionally, for each identified event, the temperature  $T_j$  was

normalized by the average value  $\tilde{T}_j$  within a window that spans  $\delta\ell = 2 \cdot 10^5 d_i$  and is centered around the discontinuity under study. This allows us to disentangle our observations from the effects of transients such as heliospheric current sheet (HCS) crossings, usually associated with minima in solar wind temperature (Suess et al. 2009; Shi et al. 2022), switchback patches observed to enhance the solar wind temperature (Shi et al. 2022), etc. Additionally, it enables us to get a more direct estimate of the relative contribution of CSs to the internal energy of the charged particle species under investigation.

It appears that no significant proton and electron heating of the solar wind occurs at times when the magnetic field is relatively smooth, as indicated by the dip in the normalized mean temperature at lag equal to  $t = 0$  s for  $\text{PVI} \leq 1$ . Increasing the threshold value  $\theta$ , however, results in a global maximum in normalized  $T_j$  close to zero lag, suggesting that both proton and electron temperatures will rise in the vicinity of coherent structures. It can be readily seen, however, that the heating process is less pronounced in the case of the electrons, because  $T_e$  does not considerably deviate from the mean  $\tilde{T}_e$ . On the other hand, proton temperature considerably increases near CSs as illustrated in Figure 2(b), with the enhancement being progressively more obvious as we consider higher PVI thresholds. There is a distinct rate of decrease for each bin, with the steepest gradients in  $T_p$  observed around the sharpest discontinuities,  $\text{PVI} \geq 6$ .  $T_p$  remains elevated near the main event, most likely because of the clustering of coherent structures (Yordanova et al. 2021; Sioulas et al. 2022b).

## 5. Summary and Conclusions

Using observations from PSP’s first encounter with the Sun, we investigated the relationship between proton and electron heating and coherent magnetic structures in the young solar wind environment. Seeking to better understand turbulent dissipation in the vicinity of solar wind sources, we have first



identified coherent structures in our data set using the PVI method (Greco et al. 2008). Subsequently, the effect of CSs on the heating of electrons and protons was examined. The electron temperature here is obtained from QTN spectroscopy (Moncuquet et al. 2020), which indicates the temperature of the distribution's core.

Our preliminary analysis corroborates previous theoretical and observational works (Osman et al. 2012; Greco et al. 2012; Servidio et al. 2012; Sorriso-Valvo et al. 2019; Qudsi et al. 2020; Yordanova et al. 2021; Sioulas et al. 2022b) and indicates that coherent structures can provide a channel for ion heating in the young solar wind. However, enhancements in electron temperature are considerably less significant, and it would be challenging to imagine that intermittent heating could account for the nonadiabatic cooling profile of electrons in the solar wind. Qualitatively, the results are consistent with what numerical works have indicated in the past, namely, enhanced heating of ions compared to electrons in the vicinity of coherent structures. (see, e.g., Parashar & Matthaeus 2016). One possible explanation for the preferential intermittent heating of protons over electrons is the "helicity barrier" mechanism that prevents turbulence energy cascade to electron scales so it can effectively heat the electrons (Squire et al. 2022). In the case where the system is continuously driven, the large-scale energy will grow in time as the parallel correlation length decreases (Meyrand et al. 2021). It is through this growth that turbulent energy is eventually funneled into a spectrum of high-frequency ion-cyclotron waves (ICWs), which end up primarily heating the ions.

As a result of our study, we gained a better understanding of how turbulent dissipation and heating of electrons and protons occur in the near-Sun solar wind environment. The main finding of this study is that proton heating from coherent structures in the nascent solar wind is preferred over electron heating. However, our results present only a preliminary comparison of electron and proton heating in the near-Sun solar wind. A complete understanding of how particle heating and dissipation occur at inertial and kinetic scales will require a more thorough statistical analysis considering a larger and higher-resolution data set. Additionally, strahl and halo components of the electron distribution function will need to be studied to provide a more complete understanding of how different electron populations behave in the vicinity of CSs.

Our results will guide future works that model the heating of the solar corona and the nascent solar wind environment. Our results will guide future works that model the heating of the nascent solar wind environment.

This research was funded in part by the FIELDS experiment on the Parker Solar Probe spacecraft, designed and developed under NASA contract NNN06AA01C; the NASA Parker Solar Probe Observatory Scientist grant NNX15AF34G; and the HERMES DRIVE NASA Science Center grant No. 80NSSC20K0604. The instruments of PSP were designed and developed under NASA contract NNN06AA01C. We thank the PSP SWEAP team led by J. Kasper and the FIELDS team led by S. Bale for use of data.

#### ORCID iDs

Nikos Sioulas  <https://orcid.org/0000-0002-1128-9685>  
 Chen Shi (时辰)  <https://orcid.org/0000-0002-2582-7085>  
 Zesen Huang (黄泽森)  <https://orcid.org/0000-0001-9570-5975>  
 Marco Velli  <https://orcid.org/0000-0002-2381-3106>

#### References

- Bale, S. D., Goetz, K., Harvey, P. R., et al. 2016, *SSRv*, 204, 49  
 Bandopadhyay, R., Matthaeus, W. H., Parashar, T. N., et al. 2020, *ApJS*, 246, 61  
 Boldyrev, S., Forest, C., & Egedal, J. 2020, *PNAS*, 117, 9232  
 Borovsky, J. E. 2021, *FrASS*, 8, 131  
 Bourouaine, S., Alexandrova, O., Marsch, E., & Maksimovic, M. 2012, *ApJ*, 749, 102  
 Bourouaine, S., & Chandran, B. D. G. 2013, *ApJ*, 774, 96  
 Bowen, T. A., Bale, S. D., Bonnell, J. W., et al. 2020, *JGRA*, 125, e2020JA027813  
 Chandran, B. D. G., Li, B., Rogers, B. N., Quataert, E., & Germaschewski, K. 2010, *ApJ*, 720, 503  
 Chasapis, A., Retinò, A., Sahraoui, F., et al. 2015, *ApJL*, 804, L1  
 Chhiber, R., Goldstein, M. L., Maruca, B. A., et al. 2020, *ApJS*, 246, 31  
 Coleman, P. J. J. 1968, *ApJ*, 153, 371  
 Fox, N. J., Velli, M. C., Bale, S. D., et al. 2016, *SSRv*, 204, 7  
 González, C. A., Tenerani, A., Matteini, L., Hellinger, P., & Velli, M. 2021, *ApJL*, 914, L36  
 Greco, A., Chuychai, P., Matthaeus, W. H., Servidio, S., & Dmitruk, P. 2008, *GeoRL*, 35, L19111  
 Greco, A., Valentini, F., Servidio, S., & Matthaeus, W. H. 2012, *PhRvE*, 86, 066405  
 Gurland, J., & Tripathi, R. C. 1971, *The American Statistician*, 25, 30  
 Halekas, J. S., Whittlesey, P., Larson, D. E., et al. 2020, *ApJS*, 246, 22  
 Huba, J. 2004, NRL: Plasma Formulary Defense Technical Information Center  
 Hudson, P. 1971, *P&SS*, 19, 1693  
 Isenberg, P. A., & Hollweg, J. V. 1983, *JGR*, 88, 3923  
 Karimabadi, H., Roytershteyn, V., Wan, M., et al. 2013, *PhPI*, 20, 012303  
 Kasper, J. C., Abiad, R., Austin, G., et al. 2016, *SSRv*, 204, 131  
 Leamon, R. J., Smith, C. W., Ness, N. F., & Wong, H. K. 1999, *JGR*, 104, 22331  
 Maksimovic, M., Zouganelis, I., Chaufray, J. Y., et al. 2005, *JGRA*, 110, A09104  
 Matthaeus, W. H., & Lamkin, S. L. 1986, *PhFI*, 29, 2513  
 Matthaeus, W. H., & Velli, M. 2011, *SSRv*, 160, 145  
 Matthaeus, W. H., Wan, M., Servidio, S., et al. 2015, *RSPTA*, 373, 20140154  
 Meyrand, R., Squire, J., Schekochihin, A. A., & Dorland, W. 2021, *JPIPH*, 87, 535870301  
 Moncuquet, M., Meyer-Vernet, N., Issautier, K., et al. 2020, *ApJS*, 246, 44  
 Osman, K. T., Matthaeus, W. H., Wan, M., & Rappazzo, A. F. 2012, *PhRvL*, 108, 261102  
 Parashar, T. N., & Matthaeus, W. H. 2016, *ApJ*, 832, 57  
 Parashar, T. N., Shay, M. A., Cassak, P. A., & Matthaeus, W. H. 2009, *PhPI*, 16, 032310  
 Parashar, T. N., Goldstein, M. L., Maruca, B. A., et al. 2020, *ApJS*, 246, 58  
 Qudsi, R. A., Maruca, B. A., Matthaeus, W. H., et al. 2020, *ApJS*, 246, 46  
 Richardson, J. D., Paularena, K. I., Lazarus, A. J., & Belcher, J. W. 1995, *GeoRL*, 22, 325  
 Servidio, S., Matthaeus, W. H., Shay, M. A., Cassak, P. A., & Dmitruk, P. 2009, *PhRvL*, 102, 115003  
 Servidio, S., Valentini, F., Califano, F., & Veltri, P. 2012, *PhRvL*, 108, 045001  
 Shi, C., Velli, M., Tenerani, A., Réville, V., & Rappazzo, F. 2022, *ApJ*, 928, 93  
 Shi, C., Panasenco, O., Velli, M., et al. 2022, *ApJ*, 934, 152  
 Sioulas, N., Isliker, H., & Vlahos, L. 2020a, *ApJL*, 895, L14  
 Sioulas, N., Isliker, H., & Vlahos, L. 2022a, *A&A*, 657, A8  
 Sioulas, N., Isliker, H., Vlahos, L., Koumtzis, A., & Pisokas, T. 2020b, *MNRAS*, 491, 3860  
 Sioulas, N., Velli, M., Chhiber, R., et al. 2022b, *ApJ*, 927, 140  
 Sioulas, N., Huang, Z., Velli, M., et al. 2022, *ApJ*, 934, 143  
 Sorriso-Valvo, L., Carbone, F., Perri, S., et al. 2018, *SoPh*, 293, 10  
 Sorriso-Valvo, L., De Vita, G., Fraternali, F., et al. 2019, *FrP*, 7, 108  
 Squire, J., Meyrand, R., Kunz, M. W., et al. 2022, *NatAs*, 6, 715  
 Stansby, D., Salem, C., Matteini, L., & Horbury, T. 2018, *SoPh*, 293, 155  
 Suess, S. T., Ko, Y. K., von Steiger, R., & Moore, R. L. 2009, *JGRA*, 114, A04103  
 Taylor, G. I. 1938, *RSPSA*, 164, 476  
 Tessein, J. A., Matthaeus, W. H., Wan, M., et al. 2013, *ApJ*, 776, L8  
 Tsurutani, B. T., & Smith, E. J. 1979, *JGRA*, 84, 2773  
 Veltri, P. 1999, *PCF*, 41, A787  
 Vlahos, L., Isliker, H., Kominis, Y., & Hizanidis, K. 2008, arXiv:0805.0419  
 Wan, M., Matthaeus, W. H., Karimabadi, H., et al. 2012, *PhRvL*, 109, 195001  
 Yordanova, E., Vörös, Z., Sorriso-Valvo, L., Dimmock, A. P., & Kilpua, E. 2021, *ApJ*, 921, 65